electronics

MDPI

Article

Signal Processing to Characterize and Evaluate Nonlinear Acoustic Signals Applied to Underwater Communications

María Campo-Valera [1,*], Dídac Diego-Tortosa [2], Ignacio Rodríguez-Rodríguez [1], Jorge Useche-Ramírez [3] and Rafael Asorey-Cacheda [4]

[1] Department of Communication Engineering, Universidad de Málaga, 29010 Málaga, Spain; ignacio.rodriguez@ic.uma.es
[2] Laboratori Nazionali del Sud, Istituto Nazionale di Fisica Nucleare, 95123 Catania, Italy; didac.diegotortosa@lns.infn.it
[3] Engineering Faculty–Sound Engineering, Universidad de San Buenaventura, Bogotá 110111, Colombia; juseche@usbbog.edu.co
[4] Department of Information and Communication Technologies, Universidad Politécnica de Cartagena, Antigones Plaza del Hospital 1, 30202 Cartagena, Spain; rafael.asorey@upct.es
* Correspondence: maria.campo@ic.uma.es

Abstract: Nonlinear acoustic signals, specifically the parametric effect, offer significant advantages over linear signals because the low frequencies generated in the medium due to the intermodulation of the emitted frequencies are highly directional and can propagate over long distances. Due to these characteristics, a detailed analysis of these signals is necessary to accurately estimate the Time of Arrival (ToA) and amplitude parameters. This is crucial for various communication applications, such as sonar and underwater location systems. The research addresses a notable gap in the literature regarding comparative methods for analyzing nonlinear acoustic signals, particularly focusing on ToA estimation and amplitude parameterization. Two types of nonlinear modulations are examined: parametric Frequency-Shift Keying (FSK) and parametric sine-sweep modulation, which correspond to narrowband and broadband signals, respectively. The first study evaluates three ToA estimation methods—threshold, power variation (Pvar), and cross-correlation methods for the modulations in question. Following ToA estimation, the amplitude of the received signals is analyzed using acoustic signal processing techniques such as time-domain, frequency-domain, and cross-correlation methods. The practical application is validated through controlled laboratory experiments, which confirm the robustness and effectiveness of the existing methods proposed under study for nonlinear (parametric) acoustic signals.

Keywords: acoustic signal processing; time of arrival (ToA) estimation; ultrasound; underwater acoustic communication; modulation; nonlinear acoustic; sensor; parametric effect

check for updates

Citation: Campo-Valera, M.; Diego-Tortosa, D.; Rodríguez-Rodríguez, I.; Useche-Ramírez, J.; Asorey-Cacheda, R. Signal Processing to Characterize and Evaluate Nonlinear Acoustic Signals Applied to Underwater Communications. *Electronics* **2024**, *13*, 4192. https://doi.org/10.3390/electronics13214192

Academic Editors: Mário P. Véstias and Rui Policarpo Duarte

Received: 18 September 2024
Revised: 21 October 2024
Accepted: 24 October 2024
Published: 25 October 2024

Copyright: © 2024 by the authors. Licensee MDPI, Basel, Switzerland. This article is an open access article distributed under the terms and conditions of the Creative Commons Attribution (CC BY) license (https://creativecommons.org/licenses/by/4.0/).

1. Introduction

Underwater acoustic communication has emerged as a critical area of acoustic research due to its capacity to study the interaction processes of signals in water and its ability to leverage their properties across various applications, including marine environmental monitoring for biodiversity conservation, seafloor profiling for enhanced understanding, navigation [1–3], marine traffic control, positioning [4,5], defense, and security [6,7], among others [8,9]. However, such communication systems encounter significant challenges due to signal interference caused by multiple reflections within the medium, the presence of ambient noise, and other disturbances that impede the optimal reception of acoustic signals as they propagate.

To mitigate these adverse effects, communication techniques based on the nonlinear propagation phenomenon known as the parametric effect have been proposed. This phenomenon facilitates directional communication through the use of high-frequency (primary

frequencies) and high-intensity transducers. The nonlinear waves generated during this process induce the emergence of low-frequency (secondary frequencies) components in the medium. This approach offers several advantages, such as the ability to communicate exclusively in the desired direction and significantly reducing multiple reflections, which can degrade the quality of the communication signal.

Since the initial studies on the theory of the parametric effect by Westervelt [10,11] and Berktay [12,13], among others [14–19], nonlinear (parametric effect) processing techniques for acoustic signals have been developed [20–24]. These techniques are crucial for enhancing the reception and quality of underwater communications. This processing involves the manipulation, transformation, and representation of signals to obtain characteristics or parameters suited to specific applications, such as underwater communications and transducer calibration, among others.

Identifying the Time of Arrival (ToA) and characteristics of underwater acoustic signals is a critical and challenging task. As the signal propagates through the underwater channel, it experiences delays and is partially masked by system or ambient noise. Additionally, it is attenuated by propagation loss and the multipath effect. The received signal is interpreted relative to the location of the transmitting system, necessitating an accurate estimation of the ToA of the received signal [25].

To identify the characteristics of these signals, various processing techniques are employed to extract relevant parameters or information that may be obscured or masked in their original representation. These parameters can be used to characterize or distinguish between different signals. Techniques such as Fourier analysis, correlation methods, and adaptive filtering algorithms [26–29] are utilized to enhance the accuracy of underwater signal detection and classification.

An overview of ToA estimation methods is provided in [30–32], which can be used when there is a change in the received signal or by identifying the first arrival; the latter approach is more accurate for wideband signals when employing the cross-correlation method, as will be discussed in the following sections. In [33], narrow autocorrelation Direct Sequence Spread Spectrum (DSSS) signals are utilized to achieve better separation between channel taps. A similar approach is presented in [34], where curve fitting is applied to DSSS signals. Exploiting the fact that underwater acoustic signals are characterized by a large temporal bandwidth product, a method for estimating signal time delay using the Multiple Signal Classification (MUSIC) algorithm is discussed in [35].

Recent studies have developed methods for estimating the ToA of signals using deep learning [36], with approaches modeling ToA and Distance of Arrival (DoA) estimation as either on-grid classification [37–40] or off-grid regression [41–43], employing deep neural networks.

Although recent studies have addressed the estimation of the ToA, the current literature lacks specific comparative methods for analyzing nonlinear acoustic signals in underwater communications, particularly regarding ToA estimation and its parameterization in terms of the amplitude of the received signal. This gap highlights the need for the development and implementation of such methods. The application of these approaches is crucial, as nonlinear acoustic signals often contain critical information that cannot be directly extracted. Advanced detection techniques are essential for the accurate identification of the information embedded in these signals. This enables better discrimination of the bits in the transmitted communication signals, thereby improving the efficiency and accuracy of nonlinear underwater acoustic communications.

To address this need, this work implements and validates two studies utilizing two types of nonlinear modulations with the bit sequence [1010010110010110]: the first is parametric Frequency-Shift Keying (FSK) modulation, and the second is parametric sine-sweep modulation. The first modulation corresponds to a narrowband signal, while the second represents a broadband signal modulation that was previously developed theoretically by the authors of [44].

1. The first study involves three methods of acoustic signal analysis for estimating the ToA: the threshold method, the power variation method (Pvar), and the cross-correlation method. For each of these methods, the accuracy and advantages relative to the Signal-to-Noise Ratio (SNR) for this type of modulation are evaluated.
2. Once the ToA has been estimated, the amplitude of the received signals is evaluated through a comprehensive analysis using time-domain, frequency-domain, and cross-correlation signal processing techniques. For each of these techniques, relevant parameters, such as voltage, are extracted for the proposed modulations.

Additionally, the practicality and robustness of these studies have been assessed through experiments conducted in a controlled laboratory environment. These experiments validate the effectiveness of the proposed methods, providing a solid foundation for their practical applications.

The paper is organized as follows: Section 2 presents the theoretical description of the first proposed study, which covers three methods used to estimate the ToA: the threshold method, the Pvar method, and the cross-correlation method. Theoretical examples are included to facilitate understanding. Section 3 develops the second study of the research, focusing on the detection of the amplitude of the received signals using time-domain, frequency-domain, and cross-correlation methods. Section 4 details the experimental setup and measurement configuration for accurate signal evaluation in water. Section 5 presents, discusses, and contrasts the results obtained from experimental measurements with the previously mentioned theoretical models. Finally, Section 6 provides final observations and conclusions of the study.

2. Methods for Estimation the Time of Arrival of Acoustic Signals

When an acoustic signal is recorded, it is crucial to conduct a thorough analysis to extract the relevant parameters based on the specific application. The recorded signal is inevitably influenced by environmental noise, commonly referred to as background noise. Therefore, accurately determining the ToA of the signal is essential to distinguish between the signal of interest and any existing noise or interference. This distinction is fundamental in communication applications, where effectively separating the signal of interest from ambient noise is critical for ensuring reliable and efficient data transmission.

This section proposes several methods to determine the ToA in parametric signals when two transducers are facing each other. To achieve this, the mathematical expressions associated with each method are implemented analytically, and the corresponding figures are generated.

2.1. Threshold Method

The threshold method involves identifying the moment when the signal exceeds a predetermined amplitude level. This method requires a high SNR and a comprehensive analysis of the emitted signal to establish an optimal threshold, defined as the minimum signal level. A higher SNR significantly enhances the accuracy of the results, as it represents the most straightforward scenario for this method. In many cases, filtering is necessary to ensure that the signal of interest is recorded with greater precision. An example of this method can be seen in Figure 1.

As an example, the signal in Figure 1 will be used for the rest of the visual explanations of the ToA calculation.

2.2. Power Variation Method (Pvar)

The power variation method (Pvar) also requires a high SNR and effective signal filtering. This method has two variants: "Cumulative Pvar" and "Saw Pvar".

To apply the mathematical formulas $Pvar_{cum}$, and $Pvar_{sum}$, a custom analysis function was developed. This code evaluates the signal using the Pvar-transform within a specific time window, detecting changes in the slope of the transformed signal. Appendix C provides a detailed breakdown of the operation.

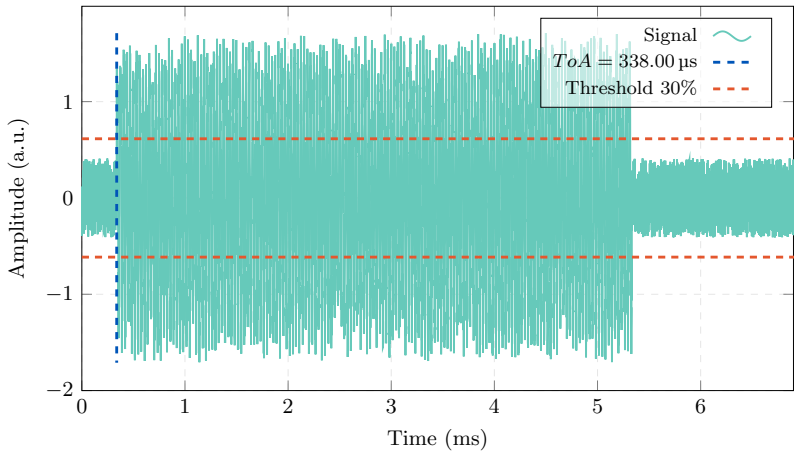


Figure 1. Example of the ToA estimation using the threshold method on a simulated signal with a SNR of 10 dB. The distance between the emitter and receiver is 0.5 m and the speed of sound in water is approximately 1480 m/s, so the expected ToA is 336.00 µs. Due to the SNR conditions, the estimated ToA by the threshold method is 338.00 µs. The 30 % threshold level is calculated on the maximum level of the signal.

The experimental case demonstrating this method can be seen in Figure 9a,b, where the ToA detection is applied to real-world signals.

The intersection point between two slopes is then calculated, corresponding to the estimated ToA.

2.2.1. Cumulative Power Variation ($Pvar_{cum}$)

The cumulative power variation method calculates the cumulative sum of the absolute values of the recorded waveform's amplitude [45], as shown in Equation (1). This method reveals an increasing trend in values, with a noticeable change in slope when the signal to be detected appears. By adjusting a specific factor, the steepness of the slope can be increased, making the identification of the ToA easier. An example of this is shown in Figure 2.

$$Pvar_{cum}[n] = \frac{\sum_{i=1}^{n} x_i^k}{\sum x[n]^k} \tag{1}$$

where k represents the power to which each data point x_i is raised, and N represents the total number of data points in the dataset.

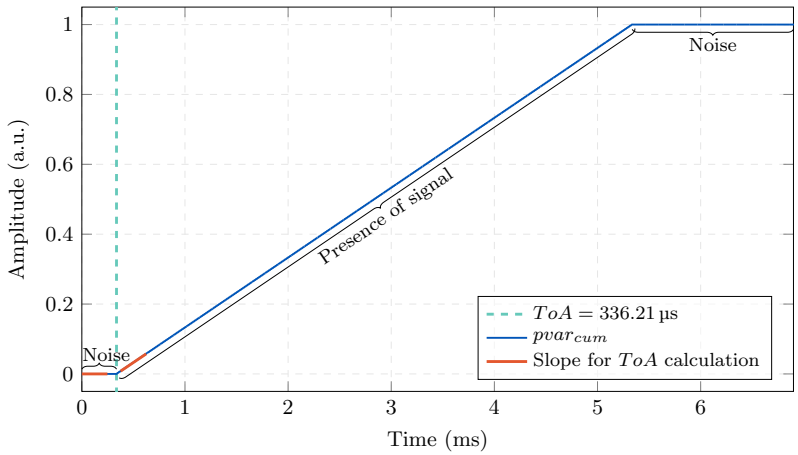


Figure 2. Scheme for the ToA estimation using the $Pvar_{cum}$ method in an ideal signal (no noise). The periods of noise (no signal) and the presence of signal are indicated, as well as the two slopes that the algorithm has considered for the calculation of the ToA (where they intersect), the ToA is 336.21 µs.

2.2.2. Saw Pvar ($Pvar_{saw}$)

The Saw Pvar method subtracts the mean value of the recorded waveform from $Pvar_{cum}$ (1), resulting in a sawtooth-like signal that accounts for the contribution of background noise, potentially eliminating the need for additional filtering. The ToA of the signal corresponds to the initial change in slope observed in $Pvar_{saw}$, as illustrated in Figure 3.

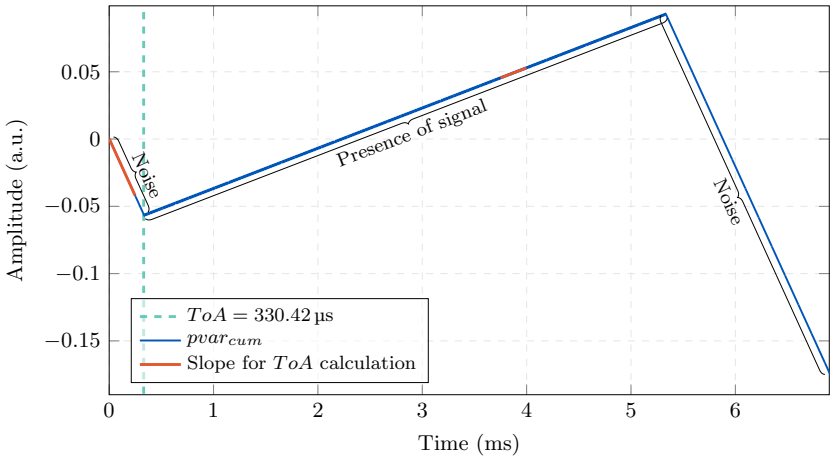


Figure 3. Scheme for the ToA estimation using the $Pvar_{saw}$ method in an ideal signal (no noise). The periods of noise (no signal) and the presence of signal are indicated, as well as the two slopes that the algorithm has considered for the calculation of the ToA (where they intersect), the ToA $Pvar_{saw}$ is 330.42 µs.

$Pvar_{saw}$ can be obtained as follows [46]:

$$Pvar_{saw}[n] = Pvar_{cum}[n] - Noise[n] \tag{2}$$

$$Noise[n] = a \cdot tn + b, \tag{3}$$

where, in Equation (3), a and b represent the coefficients resulting from the linear fit of $Pvar_{cum}$, and $t[n]$ represents the time vector of the discrete-mode signal.

2.3. Cross-Correlation Method

This method analyzes the similarity between the emitted signal and the recorded waveform by generating a correlation signal [45]. The amplitude peaks of the correlation signal are higher when the two signals coincide, with the ToA corresponding to the maximum peak of the correlation signal. A key distinction from the previously described methods is that this approach is effective at low SNR and does not require additional filtering. Furthermore, it provides improved results for sine-sweep signals, as will be discussed in subsequent sections. This method is defined as [47]

$$r_{xy}[l] = \sum_{i=1}^{N} x[n]y[n+l] \tag{4}$$

Let $x[n]$ and $y[n]$ denote the signals digitized by the transmitting transducer and the hydrophone, respectively. In this context, let $l = 1, 2, \ldots, N$ represent the number of samples by which y is delayed relative to x. The cross-correlation method involves computing the cross-correlation function for a range of delay values l. The delay time estimate is then determined as the value of l that maximizes the cross-correlation function.

An example of this is shown in Figure 4.

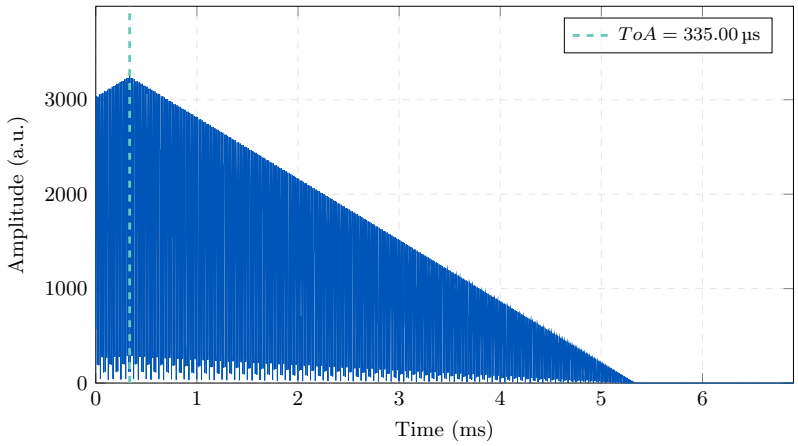


Figure 4. Example of the ToA estimation using the cross-correlation method in an ideal signal (no noise). This signal is the result of correlating a transmitted signal with a received signal, the ToA is 335.00 µs.

3. Amplitude Analysis of the Received Signal

Once the ToA of the signal at the receiver is determined, its amplitude can be analyzed. This analysis is conducted through three methods: time-domain (*Time parameterization*), frequency-domain (*Frequency parameterization*), and cross-correlation (*Cross-correlation parameterization*). Each technique is described below, highlighting the specific information it provides about the received signal, which is measured in Volts (V) in this work.

3.1. Time Parameterization

Time parameterization describes the behavior of a signal with respect to time. Time is the inherent domain of any acoustic signal, and although it is the most basic representation, and can be obtained using appropriate tools and measurement conditions, it can still be used to extract relevant information from the signal.

In the discrete time domain, the value of the signal or function is known only at specific instants along the time axis, and its amplitudes are discretized, meaning they cannot take any value but are limited to those defined by the bit depth of quantization. Therefore, the signals are digitized before processing and consist of a sequence of N samples taken at regular intervals separated by a period $T = 1/f_s$, where f_s is the sampling frequency.

In the context of this work, it is useful to know the signal parameters at certain frequencies and/or frequency bands. To obtain such information in the time domain, the basic tool used is filtering, a process that separates the useful or necessary part of a signal from other unwanted frequency components. By filtering the signal, its time profile for that frequency range is obtained, revealing only the amplitude corresponding to the desired bandwidth.

In digital processing of analyzed acoustic signals, filtering serves two primary purposes:

1. To remove unwanted noise from the received signals, specifically filtering out frequency components outside the desired range.
2. To analyze information across different frequency bands within the target frequency range.

Signals in the time domain can be described using amplitude parameters such as peak, peak-to-peak, or root mean square (rms). In this work, to compare amplitudes across different analysis domains, the peak value, $V_{p,\text{time}}$, is used. For stationary harmonic signals, this peak value can be estimated as [48]

$$V_{p,\text{time}}\{x[n]\} = V_{rms,\text{time}}\{x[n]\} \cdot \sqrt{2}, \tag{5}$$

where $V_{rms,\text{time}}$ is the value of the signal, defined as follows [48]:

$$V_{rms,\text{time}}\{x[n]\} = \sqrt{\frac{1}{N}\sum_{i=1}^{N} x_i^2[n]} \tag{6}$$

Figure 5 shows an example of the peak voltage, $V_{p,\text{time}}$, and rms voltage, $V_{rms,\text{time}}$, values obtained from a given frequency band signal.

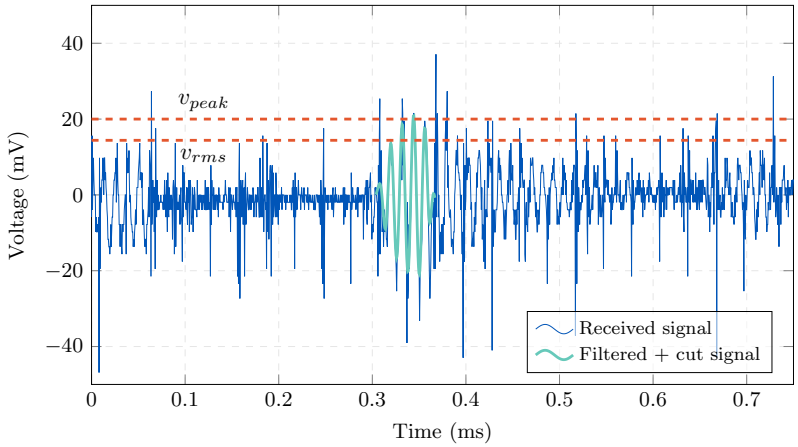


Figure 5. Example of the time domain amplitude estimation, where $V_{p,\text{time}}$ is 20 mV and $V_{rms,\text{time}}$ is 14.14 mV for the filtered and clipped received signal.

Before filtering the signal to extract information in the time domain, the received signal is trimmed to the time interval where it is assumed to be stationary.

3.2. Frequency Parameterization

The Fourier Transform $X_F(f)$ converts a signal from the time domain to the frequency domain. It is a widely used technique for analyzing stationary signals, providing the spectral characteristics of one or more frequencies without altering their content.

In the Fourier Transform, the signal is interpreted as a superposition of sine waves with periodic amplitude, constant frequency, and phase, i.e., harmonic components. The relationship between the original signal in the time domain, $x(t)$, and the signal in the frequency domain, $X(f)$, is given by the following expressions [49,50]:

$$X_F(f) = \frac{1}{\sqrt{2\pi}}\int_{-\infty}^{\infty} x(t)\cdot e^{-j2\pi ft}dt \Leftrightarrow x(t) = \frac{1}{\sqrt{2\pi}}\int_{-\infty}^{\infty} X_F(f)\cdot e^{+j2\pi ft}df \tag{7}$$

In the case of discrete signals, such as those analyzed in this work, the Discrete Fourier Transform (DFT) transforms a set of values obtained by sampling N, the continuous signal $x[n]$ to be transformed into the discrete frequency domain represented by k. This transformation is given by [51]

$$X[n] = \sum_{k=0}^{N-1} x[k]e^{\frac{-2\pi kn}{N}} \tag{8}$$

The amplitude from the frequency method is determined by analyzing the energy of the signal within a specified frequency range. Initially, the signal is transformed from the time domain to the frequency domain using the FFT, which provides information about the signal's frequency components [50]. The amplitude at a specific frequency is then calculated based on the corresponding value in the frequency spectrum. If a range of frequencies is specified, the amplitudes across that range are summed to yield a total amplitude value, $V_{p,\text{freq}}$.

3.3. Cross-Correlation Parameterization

The cross-correlation method can locate the onset of the signal in time, but does not directly provide the amplitude value in original units, such as volts or pascals. However, studies have shown that this amplitude value can be estimated from the peak of the cross-correlation between the received signal and the reference signal. If the amplitude of the transmitted signal, $V_{p,\text{send}}$, the number of samples, N_{send}, and the maximum value of the correlation between the received and transmitted signal, $V_{\text{max, corr}}$ (located at the instant of detection), are known, the peak amplitude voltage of the received signal can be estimated using the following expression [52]:

$$V_{p,\text{corr}}\left[y_{rec}\right] = \frac{2V_{\text{max, corr}}}{V_{p,\text{send}} \cdot N_{send}} \tag{9}$$

This contrasts with the time and frequency domains, where the information is based on sections of the signal. In correlation, the amplitudes of the resulting signal indicate how similar two signals are (the signal of interest compared to a reference signal with which it is correlated). This results in a time-domain representation where the amplitude of these peaks provides an identification or characteristic of the signal, showing where these peaks occur relative to the time origin of the transmitted signal. An example of this is shown in Figure 6.

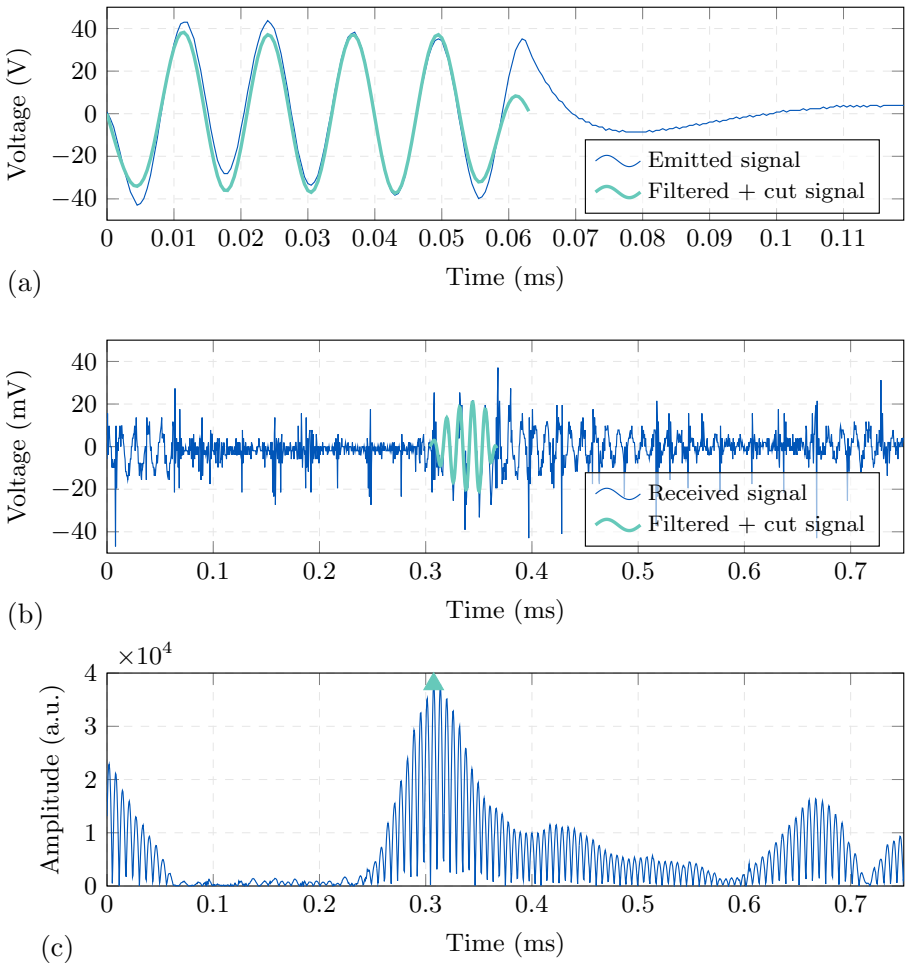


Figure 6. Amplitude estimation by the cross-correlation method. (**a**) Signal to be correlated; (**b**) received signal with a $f_s = 20\,\text{MHz}$; (**c**) cross-correlation result where $V_{p,\text{corr}}[y_{rec}]$ is 19.5 mV.

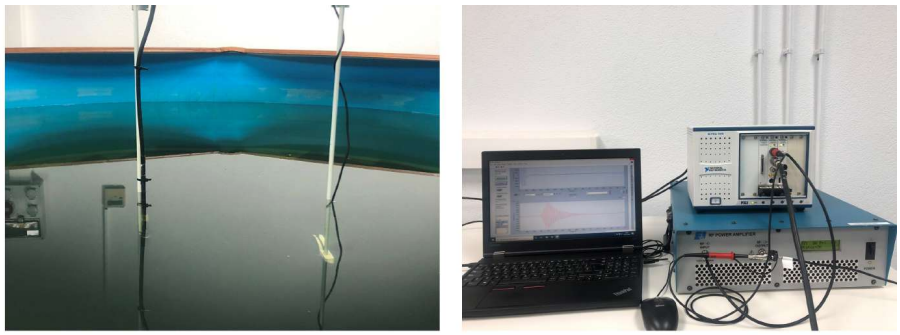
4. Experimental Set-Up

This section describes the setup used for experimental measurements in a cylindrical pool with an approximate volume of 19 m^3. The Airmar P19 transducer, with an emission sensitivity of 167 dB (re 1 µPa/V at 1 m) and a resonance frequency of 200 kHz, is used as the emitter. The Reson TC4040 transducer, with a receiver sensitivity of −206 dB (re 1 V/µPa at 1 m) within its frequency bandwidth, serves as the receiver. The distance between the two transducers is approximately 32 cm.

Figure 7 illustrates the experimental setup and connection configuration for calibration. The E&I 1040L amplifier, along with the data generation and acquisition system comprising a National Instruments PXI-1073 chassis, PXIe-5433 generator card, and PXIe-5122 oscilloscope, is controlled by a laptop via the NI PXI ExpressCard-8360. Additionally, a TES TECT HV series x100 attenuator probe is used to attenuate the signal at the amplifier output, allowing it to be recorded by the PXI system.

No hardware measurement system is ideal, as all introduce some electromechanical delay, however small, into the received signal. To mitigate this problem, high-quality commercial equipment that is characterized and calibrated in the laboratory is essential. These devices provide delay values to be considered in the analysis and are designed to minimize noise and increase SNR, thereby improving the accuracy of the ToA methods presented in this study.

In real-world environments where the receiver operates independently of the transmitter, synchronization of both devices using a common reference, such as Global Positioning System (GPS), is critical for accurate ToA measurements. However, if the primary objective is to detect signals containing information (bit strings), synchronization may not be necessary; once detected, these signals can be "read" based on the internal clock of the receiving system, whether it is Coordinated Universal Time (UTC) or not. However, if an accurate ToA is required for further analysis, the reliability of the results will depend on the level of synchronization achieved between the systems.



(**a**) (**b**)

Figure 7. Experimental set-up for signals in a laboratory pool. (**a**) On the right, the AIRMAR P19 as emitter, and on the left, the RESON TC4040 hydrophone receiver distanced 32 cm apart; (**b**) devices and connections used: computer, PXI, and amplifier.

Figure 8 shows a block diagram of the experimental setup used in the measurements.

The measurements were performed using the NI PXIe 5433 function generator, which is connected to the PC and uses LabVIEW to send the user-selected signal to the input of the E&I 1040L RF amplifier. The amplifier boosts the signal and transmits it through its output to a piezoelectric transducer. Additionally, a probe connected to the amplifier output attenuates the signal by a factor of 100 so that it can be recorded at the PXI input through channel 0 (ch. 0). The pressure waves propagating through the water are received by the hydrophone, converted into an electrical signal, and recorded at the input of channel 1 (ch. 1) of the PXI. The LabVIEW program generates files for the transmitted and received signals, which are analyzed using MATLAB software R2023a.

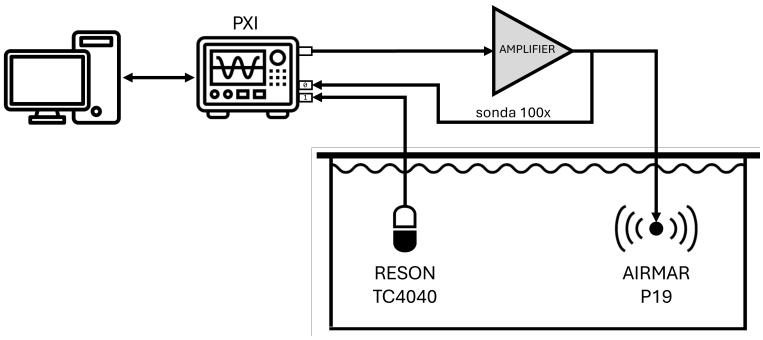


Figure 8. Block diagram of the laboratory pool measurement setup.

5. Analysis and Results of the Nonlinear Modulated Signals

In the analysis of the studied signals, two types of parametric modulations used in underwater acoustic communications are proposed: (i) Frequency-Shift Keying (FSK) and (ii) sine-sweep modulation, as explained theoretically in [53,54], respectively. The carrier signal for each measurement was defined as $\omega_c = \sin(2\pi f_c t)$, where the carrier frequency f_c was 200 kHz, and the sampling frequency f_s was 20 Ms/s.

The experimental results for the parametric modulations tested in the laboratory pool are presented, where a binary message [1010010110010110] was transmitted with the transducers facing each other at an approximate distance of 32 cm. Three methods for obtaining the ToA were studied: the threshold, Pvar, and cross-correlation methods. Additionally, their amplitude parameterization in the time and frequency domains, as well as the cross-correlation method discussed in Section 2, were analyzed.

Since the proposed modulations have been theoretically explained in [53,54], they will be briefly summarized in this paper.

5.1. Frequency-Shift Keying (FSK) Modulation

Parametrically, this modulation can be achieved using two modulating signals, f_{m1} and f_{m2}, with frequencies that are half of the frequencies associated with each bit to be received ($f_{m1} = f_{bit1}/2$ for bit '1', and $f_{m2} = f_{bit0}/2$ for bit '0'). The alternation between these frequencies represents the corresponding bit changes until the desired binary code is reproduced. Using this nonlinear technique of modulating a carrier with FSK results in another FSK signal at twice the frequency (secondary frequency) [53].

The parametric expression for FSK modulation is given in Equation (10) [53],

$$\begin{aligned} x_{bit1}(t) &= AE_{FSK_{bit1}}(t) \cdot \omega_c,\ t = t_{bit1} \\ x_{bit0}(t) &= AE_{FSK_{bit0}}(t) \cdot \omega_c,\ t = t_{bit0}, \end{aligned} \tag{10}$$

where $x_{bit1,bit0}$ is the FSK modulated signal (primary frequency) for each bit, defined as the product of the modulating signal $E(t) = \sin(2\pi f_m t)$ and the carrier signal $\omega_c = \sin(2\pi f_c t)$. Here, A represents the amplitude of the modulated signal, and t is the time for each bit.

FSK modulation is proposed with two modulating frequencies, f_{m1} = 20 kHz and f_{m2} = 15 kHz, each with a duration of 1 ms per bit. This modulation is expected to generate a parametric signal at twice the frequency, specifically 40 kHz for f_{m1} and 30 kHz for f_{m2}.

5.2. Sine-Sweep Modulation

Sine-sweep nonlinear modulation is a type of broadband signal modulation where bit '1' is represented by an upward sine-sweep from f_{m1} to f_{m2} (Equation (11)) over time, and bit '0' by a downward sine-sweep from f_{m2} to f_{m1} (Equation (12)). To derive these expressions parametrically, it is important to note that the modulating signal will be half the frequency of the parametric signal, as discussed in [44]. The desired bit sequence is generated by concatenating the individual bits, as follows [44]:

$$E_{uss}(t) = \sin\left[\left(\frac{\omega_{m1}+\omega_{m2}}{\tau_{ss}}\,t+\omega_{m1}\right)t\right], 0 \le t \le \tau_{ss}, \tag{11}$$

$$E_{dss}(t) = \sin\left[\left(\frac{\omega_{m2}-\omega_{m1}}{\tau_{ss}}\,(t-\tau_{ss})+\omega_{m1}\right)(t-\tau_{ss})\right], 0 \le t \le \tau_{ss}, \tag{12}$$

where τ_{ss} is the bit duration.

In the experiments, a sine-sweep modulation ranging from 5 kHz to 25 kHz is proposed, with a duration of 1 ms per bit. Additionally, a carrier frequency $f_c = 200$ kHz is used. It is expected that this modulation will generate a parametric signal (secondary frequency) at twice the frequency, specifically in the range of 10 kHz to 50 kHz.

5.3. Signal Processing for ToA Estimation

Since both proposed modulations were measured at a distance of 30 cm for sine-sweep modulation and 32 cm for the FSK modulation between transducers, only the ToA results for the sine-sweep modulation are presented in Figure 9. The ToA results for both modulations are detailed in Table 1.

Appendix A provides a flowchart for a better understanding of the signal processing to the ToA estimation.

Once the sine-sweep modulation, ranging from 5 kHz to 25 kHz with a bit duration of 1 ms, was measured in the laboratory pool with a distance of 30 cm between the transducers, the ToA of the received signal, concatenated with the bit sequence [1010010110010110], was estimated.

Figure 9 shows that the ToA aligns with the three methods studied in Section 2. For the threshold method, the ToA is 232.6 µs, with the threshold set at 30% of the maximum value of the received signal. Given the high SNR is around 7.8 dB, this threshold is adequate for accurate detection. The ToA obtained using the $Pvar_{cum}$ method is 241.32 µs and $Pvar_{saw}$ is 241.43 µs. The maximum peak obtained by correlating the received signal with the transmitted signal establishes the ToA of the received signal, with a value of 231.0 µs. These results confirm the consistency of the methods and enable the next step: bit detection and amplitude parameterization. This analysis is conducted in the time domain, the frequency domain, and using the cross-correlation method.

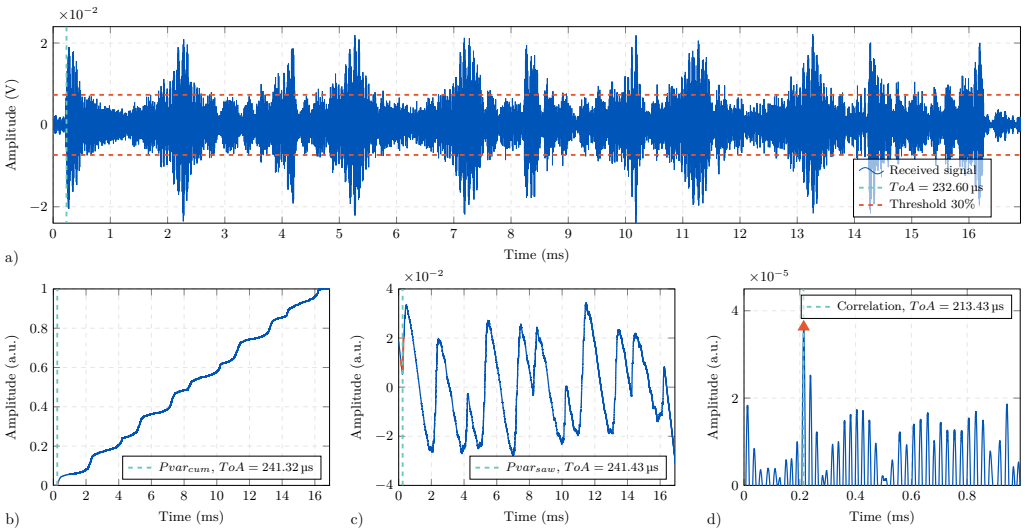


Figure 9. ToA estimation for the sine-sweep received signal concatenated with the bit sequence [1010010110010110]. (**a**) Using the threshold method; (**b**) using the $Pvar_{cum}$ method; (**c**) using the $Pvar_{saw}$ method; (**d**) zoom in close to the ToA estimated by the cross-correlation method.

Table 1 shows the ToA results for both the FSK and sine-sweep modulation. A total of five measurements were taken, with their mean and standard deviation calculated.

These values are crucial for evaluating the accuracy and repeatability of the methods used, providing a solid foundation for validating the communication system within the controlled environment (a laboratory pool).

For a distance between transmitter and receiver of 32 cm and the speed of sound in water of approximately 1480 m/s, a ToA= 216.2 µs is expected, so that the ToA threshold is the closest to this value, as shown in Table 1. However, the cross-correlation method is particularly effective for signal analysis under high SNR conditions. When the SNR is high, cross-correlation facilitates the accurate identification of the arrival times of each bit, significantly improving temporal resolution and reducing errors associated with interference or noise. This behavior allows for more precise ToA estimations, which is crucial in applications where temporal accuracy is essential, such as in the transmission and reception of parametric nonlinear acoustic signals.

Table 1. Estimated ToAs for the received signal using the threshold, Pvar, and cross-correlation methods in the FSK and sine-sweep modulations.

ToA Estimation Methods	FSK Modulation	Sine-Sweep Modulation
	Mean	Mean
Threshold	(218.43 ± 2.97) µs	(232.6 ± 3.45) µs
$Pvar_{cum}$	(219.31 ± 2.93) µs	(241.32 ± 3.65) µs
$Pvar_{saw}$	(219.31 ± 2.93) µs	(241.43 ± 3.50) µs
Cross-correlation	(220.23 ± 1.39) µs	(229.35 ± 2.94) µs

5.4. Amplitude Parameterization and Bit Detection of the Proposed Modulations.

When a medium is excited by a high-amplitude signal (primary frequency), mutual interaction between the waves occurs due to the nonlinear effects of the channel. This interaction leads to the formation of secondary waves with frequencies that are linear combinations of the sum $\omega_s = \omega_a + \omega_b$, and the difference $\omega_d = \omega_a - \omega_b$ of the primary frequencies (signals sent), where ω_a and ω_b are the harmonics corresponding to the primary frequency. Additionally, the dissipative effects of the medium attenuate the higher-frequency waves, eventually causing them to disappear. At large distances from the source, a single frequency signal corresponding to ω_d prevails. Since ω_d is a low frequency, it undergoes less attenuation and can propagate over greater distances. This phenomenon, known as the parametric effect, generates highly directional low-frequency signals [55,56].

The low amplitude of the difference-frequency signal, ω_d, generated by the parametric effect presents a significant challenge for detection in noisy environments, as this signal tends to be masked by background noise. This highlights the importance of employing advanced signal processing techniques to extract and analyze such low-intensity signals, ensuring accurate and reliable detection.

After estimating the ToA for the studied modulated signals, a comprehensive approach involves analyzing the spectrogram of the recorded modulations to confirm the presence of the parametric effect. Figure 10 illustrates the Power Spectral Density (PSD) for both FSK and sine-sweep modulations. The emitted signal around 200 kHz is highlighted, along with the parametric FSK signal with $f_{m1} = 20$ kHz and $f_{m2} = 15$ kHz, and the sine-sweep modulation exhibiting upward and downward sweeps from 5 kHz to 25 kHz. These frequency variations, which are associated with the parametric effect, are distinctly visible.

The results obtained from this experiment not only corroborate the underlying theory, but also show that the frequencies generated by the parametric effect are twice the frequencies of the original signals. This behavior is consistent with the theory of parametric signal generation, where the nonlinear interaction between high-frequency waves generates lower-frequency components [57].

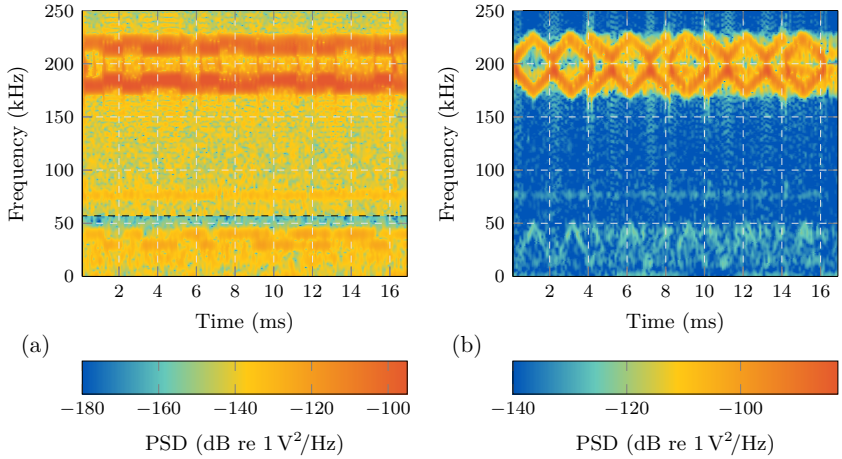


Figure 10. Spectrogram of the received signal using 4096 samples for the FFT with 50% overlap. (**a**) Parametric FSK modulation (high frequencies), with a Butterworth low-pass filter of order 6 applied for better visualization of low frequencies (the dotted line differentiates between the two analyses). Around 200 kHz, the primary frequency is observed, and the bits in 30 kHz and 40 kHz represent the low frequency parametric signal (secondary frequencies); (**b**) parametric sine-sweep modulation. Around 200 kHz, the primary frequency is observed, and between 10 kHz to 50 kHz the low frequency parametric signal (secondary frequencies).

Once the parametrically generated acoustic signal is obtained, its amplitude is parameterized in both the time and frequency domains, as well as using the cross-correlation method. However, in the analyses performed, filtering the parametric signal at low frequencies and processing it in the time domain does not reveal any variation in the bit amplitudes. Therefore, the only way to determine the amplitude value for each bit is through the application of the cross-correlation method. Nevertheless, the peak voltage and rms value in the time domain, as well as the peak voltage in the frequency domain for the primary frequency, are obtained, as illustrated in Figure 11. Appendix B provides a detailed understanding of the step-by-step procedure for processing both the primary frequency and the secondary (parametric) frequency.

In relation to Figure 11a, for the primary frequency of the FSK modulation, a $V_{p,\text{time}}$ and $V_{rms,\text{time}}$ range of (3.11 ± 0.15) mV and (2.02 ± 0.11) mV, respectively, are observed, along with a $V_{p,\text{freq}}$ range of (0.95 ± 0.43) mV, for bit '1'. In contrast, for bit '0', the observed $V_{p,\text{time}}$ and $V_{rms,\text{time}}$ values are (4.42 ± 0.49) mV and (3.13 ± 0.35) mV, respectively, with a $V_{p,\text{freq}}$ of (5.07 ± 0.57) mV. In general, the amplitude values for the average of bit '0' are greater than those for bit '1'. This can be explained by the fact that nonlinear signals are amplified or attenuated differently, depending on the frequency. In this context, bit '0' experiences greater gain or response in the medium due to the nonlinear characteristics of the environment. In water, energy absorption is more significant at higher frequencies than at lower ones, leading to a decrease in signal power as frequency increases. However, in a downward sweep, where higher frequencies propagate first and then transition to lower frequencies, the latter experience less absorption, resulting in a higher signal amplitude.

For the secondary or parametric frequency, the values of $V_{p,\text{freq}}$ and $V_{p,\text{corr}}$ are much smaller, in the order of µV.

In Figure 11b, for the primary frequency of the sine-sweep modulation, the values of $V_{p,\text{time}}$ and $V_{rms,\text{time}}$ are observed as (6.47 ± 0.13) mV and (4.51 ± 0.09) mV, respectively, along with a $V_{p,\text{freq}}$ of (0.43 ± 0.11) mV, for bit '1'. In contrast, for bit '0', the measured $V_{p,\text{time}}$ and $V_{rms,\text{time}}$ values are (5.96 ± 0.14) mV and (4.22 ± 0.10) mV, respectively, with a $V_{p,\text{freq}}$ of (0.44 ± 0.08) mV. Overall, for this modulation, the peak and rms voltage values are similar for bits '1' and '0'. For the secondary beam, the amplitude values in volts for bit '0' (descending sweep) are greater than those for bit '1'. Both the amplitude values in

the frequency domain and those obtained using the cross-correlation method are in the μV range.

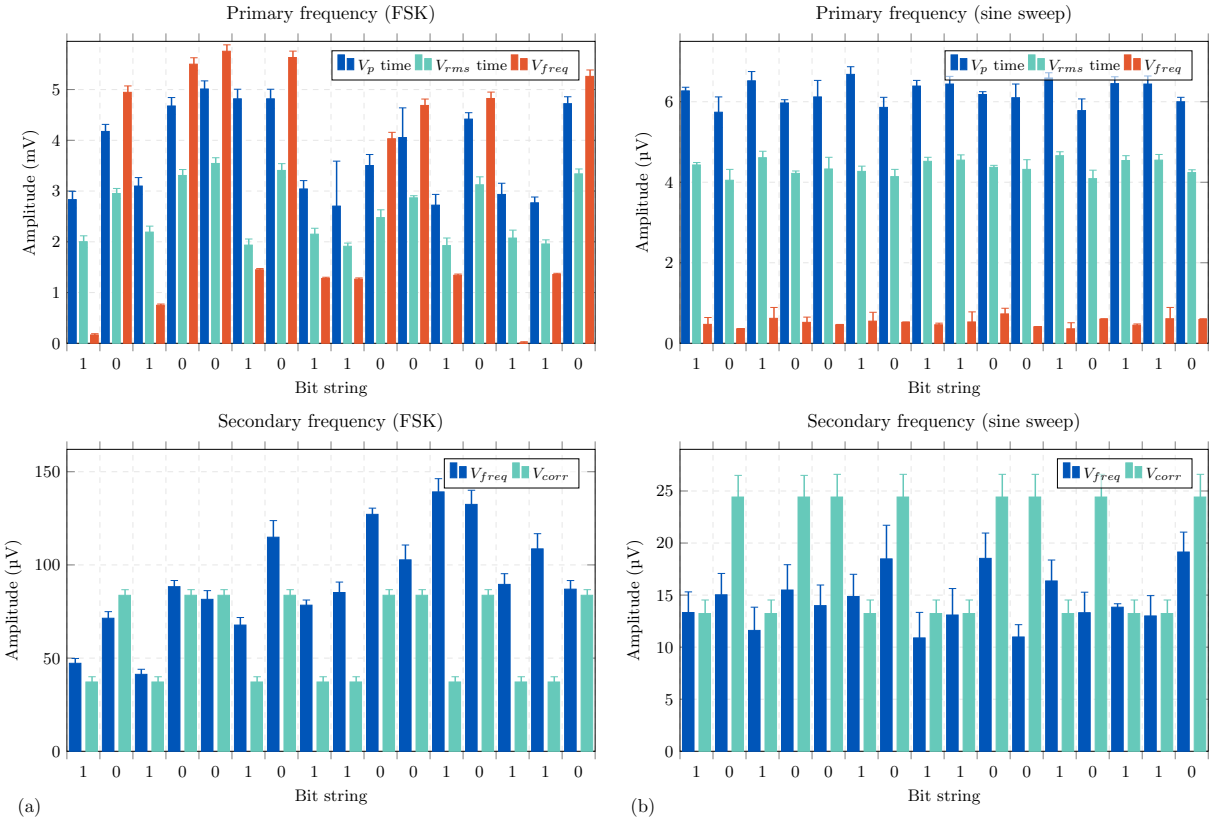


Figure 11. Amplitude values for primary and secondary frequencies (parametric signal) estimated by the different methods. (**a**) For the FSK modulation; (**b**) for the sine-weep modulation.

The parameter $V_{p,\text{freq}}$ does not work correctly in the sine-sweep technique due to the inherent property of this type of signal. A sinusoidal signal concentrates all its energy at a single frequency. Therefore, to estimate its amplitude, it is sufficient to analyze that specific frequency using the FFT, as is the case with FSK modulation (Figure 11a). In contrast, in sine-sweep modulation (Figure 11b), the energy is distributed across a range of frequencies. This complicates the control of the sine-sweep signal because the resolution of the FFT is directly related to the number of samples (NFFT) used in the transformation. Due to this distribution of energy and the limited resolution of the FFT, the calculation of $V_{p,\text{freq}}$ in sweep signals becomes inaccurate.

In systems that rely on precise frequency measurements for communication or detection, such as in underwater communications or sonar systems, such inaccuracies can affect signal quality and transmission efficiency, ultimately reducing the overall effectiveness of the system.

Bit Detection for Parametric Modulations: FSK and Sine-Sweep

Cross-correlation is a technique used to identify the presence of specific signals in a recording by employing an adapted filter. This method not only aids in detecting the occurrence of the signal, but can also be used to estimate its amplitude (Equation (9)). The technique relies on correlating a filter with an impulse response designed to match the target signal within the recording. When a match occurs, a peak is observed in the correlation function.

To illustrate the procedure, if the received signal (filtered at low frequencies for better visualization with a Butterworth filter of order 6) for bit '1' is correlated with the second derivative of the squared envelope of the transmitted bit '1' signal, an event is expected,

which will appear as a significant peak in the correlation function. This peak indicates a high similarity between the recorded signal and the expected signal for bit '1', confirming the correct detection of this bit.

Conversely, when the received signal for bit '0' is correlated with the second derivative of the squared envelope of the transmitted bit '1' signal, no significant peak should be observed. This is because the bit '0' signal should not match the reference for bit '1', resulting in no match and, consequently, no event detection.

Similarly, for detecting bit '0', the received signal for bit '0' is correlated with the second derivative of the squared envelope of the transmitted bit '0' signal. In this case, a peak is expected in the correlation function. The presence of this peak will confirm the accurate detection of bit '0'.

Figure 12 illustrates both the received signal and the resulting cross-correlation for the two bit values, using the parametric modulations FSK (Figure 12a) and sine-sweep (Figure 12b). Both correlations have been normalized to facilitate comparison. Overlaying these correlations allows for a clear visualization of the distinction between the two bits and demonstrates the ease with which this parametric effect can be detected.

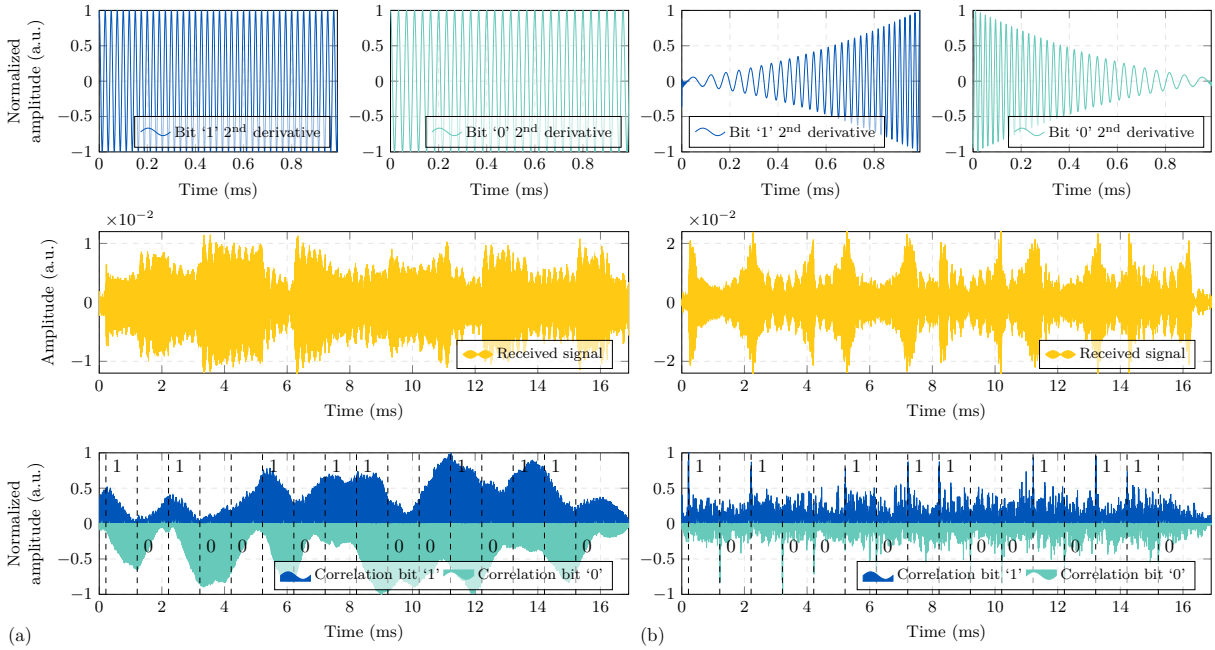


Figure 12. Detection of the bit string [1010010110010110] based on high cross-correlation peaks for each bit (bit '0' and bit '1') at the expected ToA, once the first is known. (**a**) For the FSK modulation; (**b**) for the sine-sweep modulation.

Once the ToA of the bit string is estimated, with each subsequent bit detected at 1 ms intervals. In the cross-correlations for both modulated signals, good temporal detection of each bit is observed. In Figure 12a, for FSK modulation, it is noted that the correlation peaks are quite broad (on the order of the bit duration, approximately), due to the fact that this type of modulation is essentially a pure tone that changes frequency. Correlations with narrowband signals tend to be less efficient in bit discrimination. The average amplitude in volts of the correctly detected bits '1' and '0' is 28.8 µV and 83.4 µV, respectively.

To address the limitations of the correlation peak width, which introduces some error in detecting consecutive identical bits and in estimating each bit's detection individually, Figure 12b proposes sine-sweep modulation. This modulation presents much narrower correlation peaks due to its broader spectral bandwidth. It is observed that the correlation peaks are significantly narrower compared to those with FSK modulation, and the detected bits are much clearer to discern. Regarding bit discrimination, the average amplitude in

volts of the correctly detected bits '1' and '0' at the correct instant is 59.0 µV and 66.4 µV, respectively. These results can be seen in more detail in Table 2 for both modulations.

Table 2. Amplitudes in volts for each bit in the string. The "Diff factor" refers to the difference factor between bit amplitudes calculated by the peak in the cross-correlation method.

Bit String	FSK Modulation			Sine-Sweep Modulation		
	Bit '1' (µV)	Bit '0' (µV)	Diff Factor	Bit '1' (µV)	Bit '0' (µV)	Diff Factor
1	21.1	11.3	1.9	67.3	21.9	3.07
0	35.4	68.2	19.2	12.7	68.9	5.4
1	16.5	12.1	1.35	58.8	15.2	3.8
0	2.7	91.3	33.4	16.8	83.2	4.9
0	8.3	73.6	8.8	18.7	59.4	3.2
1	31.8	15.4	2.05	52.3	31.4	1.6
0	12.5	84.5	6.74	14.4	70.3	4.8
1	27.6	27.6	1.00	58.5	20.3	2.8
1	30.3	39.8	0.76	58.9	26.2	2.2
0	15.8	101.8	6.4	13.9	65.9	4.7
0	14.5	87.4	6.02	16.3	69.9	4.3
1	42.3	65.2	0.6	62.9	15.7	4.0
0	25.6	89.6	3.5	25.4	65.8	2.6
1	29.1	36.1	0.8	64.3	16.9	3.8
1	32.0	48.8	0.6	49.6	14.0	3.5
0	99.3	70.8	7.1	15.2	47.8	3.1

The results obtained demonstrate that FSK and sine-sweep parametric modulations are viable alternatives for nonlinear underwater acoustic communications, especially when employing a wide frequency bandwidth. In particular, sine-sweep signals offer significant advantages for modulation, including low computational cost and reduced susceptibility to background noise. These characteristics make these techniques well-suited for applications where accuracy and efficiency in signal detection are crucial.

6. Conclusions

This work addressed a critical gap in the current literature by developing and validating methods for ToA estimation and amplitude parameterization of nonlinear acoustic signals in underwater communications using signal processing. The research introduces and evaluates two nonlinear modulation techniques, parametric FSK and sine-sweep modulations, using a structured bit sequence. Moreover, by combining the threshold, power variation (Pvar) and cross-correlation methods, the study demonstrates the effectiveness of these approaches in accurately estimating ToA and extracting relevant signal parameters. The results, validated through controlled laboratory experiments, provide a solid framework for improving bit detection and discrimination in nonlinear underwater acoustic communications. These advances provide a solid foundation for future research and practical applications in this area, potentially improving the reliability and efficiency of communications in underwater environments.

In terms of bit discrimination and detection using the cross-correlation method, the correlation peaks are detected quite close to the expected times, taking into account the ToA at which the signal is expected to be received. The behavior of the cross-correlation and the resulting peak width have implications for both detection and bit discrimination. In the case of FSK modulation, the narrowband nature of the signals results in relatively wide correlation peaks, which can make detection difficult. In contrast, nonlinear sine-sweep modulation has much narrower correlation peaks. This is because the signal is broadband and attenuates more rapidly, resulting in a sharper correlation amplitude and width. In addition, amplitude parameterization in both the time and frequency domains allows for the extraction of values necessary to better understand the generation of the parametric signal.

Author Contributions: Conceptualization, M.C.-V.; methodology, M.C.-V. and D.D.-T.; validation, M.C.-V., D.D.-T., I.R.-R., J.U.-R. and R.A.-C.; formal analysis, M.C.-V. and D.D.-T.; investigation, M.C.-V., D.D.-T., I.R.-R., J.U.-R. and R.A.-C.; writing—original draft preparation, M.C.-V.; writing—review and editing, M.C.-V., D.D.-T., I.R.-R., J.U.-R. and R.A.-C.; supervision, M.C.-V., D.D.-T., I.R.-R., J.U.-R. and R.A.-C. All authors have read and agreed to the published version of the manuscript.

Funding: This work was a result of the ThinkInAzul and AgroAlNext programmes, funded by Ministerio de Ciencia, Innovación y Universidades (MICIU) with funding from European Union NextGenerationEU/PRTR-C17.I1 and by Fundación Séneca with funding from Comunidad Autónoma Región de Murcia (CARM). This work was also supported by the grants PID2023-148214OB-C21 and TED2021-129336B-I00, funded by MICIU/AEI/10.13039/501100011033 and by the European Union NextGenerationEU/PRTR. This work was also funded by Fundación Séneca (22236/PDC/23). This research was also contextualized to DAIMon, a cascade funding action deriving from the Horizon Europe project aerOS, funded by the European Commission under grant number 101069732.

Data Availability Statement: The data presented in this study are available upon request from the corresponding author.

Acknowledgments: María Campo-Valera, would like to thank the Universidad de Málaga, Dídac Diego-Tortosa would like to thank the INFN Experimental Fellowship for its support through the Post-Doctoral Senior Level 3 Research Grant B.C. n. 23591/2021, which funded his position as a postdoctoral researcher. Ignacio Rodríguez-Rodríguez would like to thank Plan Andaluz de Investigación, Desarrollo e Innovación (PAIDI), Junta de Andalucía, Spain.

Conflicts of Interest: The authors declare no conflicts of interest.

Appendix A

Figure A1 illustrates the process for obtaining ToA for both the primary and secondary frequencies. To extract the primary frequency, the raw recorded signal is first processed with a sixth-order low-pass filter, with a cutoff frequency at the carrier frequency f_c = 200 Hz, plus the modulating frequency f_m. The resulting signal is multiplied by a factor of 1.05 to provide a margin greater than $f_c + f_m$. This modified signal is then used to estimate the ToA using methods such as cross-correlation, threshold, $Pvar_{cum}$, and $Pvar_{sum}$. The ToA analysis of each bit of the transmitted chain is performed independently using the cross-correlation method.

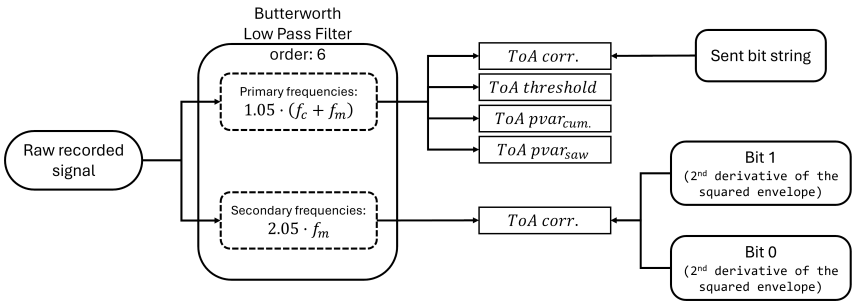


Figure A1. Flow char for obtaining the ToA for both primary and secondary frequencies (parametric signal).

For the secondary frequencies, the raw received signal is processed with a sixth-order low-pass filter, set to the modulation frequency, and multiplied by a factor of 2.05 to ensure an upper limit at the modulating frequency f_m. ToA estimation is again performed using the cross-correlation method. Additionally, the ToA of each bit is estimated by calculating the second derivative of the square envelope of the transmitted signal and correlating it with the received signal for each bit.

Appendix B

The process for Figure A2 is similar to the previous one, with the difference that in this process the amplitude values are obtained.

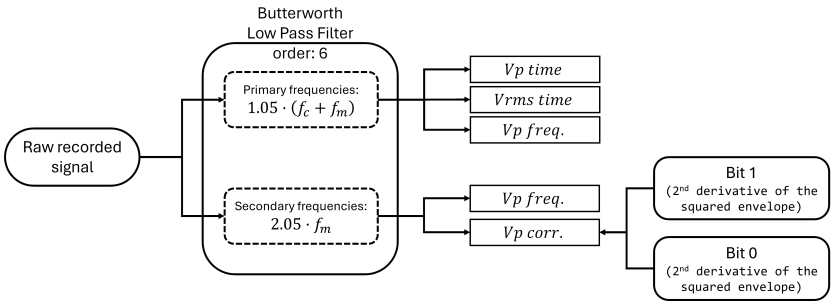


Figure A2. Flowchart for obtaining amplitude values for both primary and secondary frequencies (parametric signal).

Appendix C

Below is a detailed breakdown of how the function for the Pvar method works:

1. Signal input: The function takes as input the raw signal, the f_s, the duration of the evaluation window T_w, and the power parameter n for the Pvar method. These inputs help define the scope and resolution of the ToA analysis.
2. Pvar transform: The function computes the Pvar-transform of the signal, which is essentially the cumulative sum of the absolute value of the signal raised to the power n. This operation helps to smooth the signal and highlight key variations.
3. Slope calculation: The function then fits linear segments (slopes) to portions of the transformed signal within the time window. These slopes represent the changes in signal intensity over time and are essential for detecting the ToA.
4. Slope intersection and ToA estimation: Once the slopes are determined, the function calculates the intersection between them. This intersection corresponds to the estimated ToA, as it represents a significant change in the signal's behavior, likely caused by the arrival of the transmitted signal.
5. Noise simplification (optional): if enabled, the function includes a noise simplification step to handle noisy signals, improving the robustness of the ToA estimation in low SNR environments.
6. Parallel processing: for large datasets, the function can utilize parallel processing (via the parforMode parameter) to speed up the Pvar-transform calculations, making the function scalable for more complex scenarios.
7. Visualization: If required, the function can generate plots to visualize the signal, the Pvar-transform, and the detected ToA points. This feature can be enabled with the plotter parameter, helping to visually validate the accuracy of the ToA estimation.

References

1. Lu, J.; Zhang, H.; Li, S.; Wu, P.; Huang, W. Enhancing Few-Shot Prediction of Ocean Sound Speed Profiles through Hierarchical Long Short-Term Memory Transfer Learning. *J. Mar. Sci. Eng.* **2024**, *12*, 1041. [CrossRef]
2. Khan, M.S.; Petroni, A.; Biagi, M. Cooperative Communication Based Protocols for Underwater Wireless Sensors Networks: A Review. *Sensors* **2024**, *24*, 4248. [CrossRef] [PubMed]
3. Janowski, Ł.; Wróblewski, R. Application and Evaluation of the AI-Powered Segment Anything Model (SAM) in Seafloor Mapping: A Case Study from Puck Lagoon, Poland. *Remote Sens.* **2024**, *16*, 2638. [CrossRef]
4. Campo-Valera, M.; Asorey-Cacheda, R.; Rodríguez-Rodríguez, I.; Villó-Pérez, I. Characterization of a piezoelectric acoustic sensor fabricated for low-frequency applications: A comparative study of three methods. *Sensors* **2023**, *23*, 2742. [CrossRef]
5. Tang, N.; Zeng, Q.; Luo, D.; Xu, Q.; Hu, H. Research on development and application of underwater acoustic communication system. *J. Phys. Conf. Ser. Iop Publ.* **2020**, *1617*, 012036. [CrossRef]
6. Felis-Enguix, I.; Otero-Vega, J.; Campo-Valera, M.; Villó-Pérez, I.; Gómez-Tornero, J. Practical aspects of acoustic leaky-wave antennas applied to underwater direction finding. *Eng. Proc.* **2020**, *2*, 93. [CrossRef]
7. Hwang, Y.; Ahn, H.; Nguyen, D.N.; Kim, W.; Moon, W. An underwater parametric array source transducer composed of PZT/thin-polymer composite. *Sens. Actuators A Phys.* **2018**, *279*, 601–616. [CrossRef]
8. Bjørnø, L.; Neighbors, T.; Bradley, D. *Applied Underwater Acoustics*; Elsevier: Amsterdam, The Netherlands, 2017.
9. Murad, M.; Sheikh, A.A.; Manzoor, M.A.; Felemban, E.; Qaisar, S. A survey on current underwater acoustic sensor network applications. *Int. J. Comput. Theory Eng.* **2015**, *7*, 51. [CrossRef]

10. Westervelt, P.J. Scattering of Sound by Sound. *J. Acoust. Soc. Am.* **1957**, *29*, 199–203. [CrossRef]
11. Westervelt, P.J. Parametric Acoustic Array. *J. Acoust. Soc. Am.* **1963**, *35*, 535–537. [CrossRef]
12. Berktay, H. Possible exploitation of non-linear acoustics in underwater transmitting applications. *J. Sound Vib.* **1965**, *2*, 435–461. [CrossRef]
13. Berktay, H.; Leahy, D. Farfield performance of parametric transmitters. *J. Acoust. Soc. Am.* **1974**, *55*, 539–546. [CrossRef]
14. Villó-Pérez, I.; Alcover-Garau, P.M.; Campo-Valera, M.; Toledo-Moreo, R. A novel 1D-FDTD scheme to solve the nonlinear second-order thermoviscous hydrodynamic model. *Commun. Nonlinear Sci. Numer. Simul.* **2022**, *118*, 107015. [CrossRef]
15. Yu, S.; Liu, B.; Yu, K.; Yang, Z.; Kan, G.; Zong, L. Application of a parametric array over a mid-frequency band (4–10 kHz) –measurements of bottom backscattering strength. *Ocean. Eng.* **2023**, *280*, 114914. [CrossRef]
16. Campo-Valera, M.; Felis-Enguix, I.; Villó-Pérez, I. Signal Processing for Parametric Acoustic Sources Applied to Underwater Communication. *Sensors* **2020**, *20*, 5878. [CrossRef] [PubMed]
17. Campo-Valera, M.; Felis, I. Underwater acoustic communication for the marine environment's monitoring. *Proceedings* **2019**, *42*, 51. [CrossRef]
18. Campo-Valera, M.; Ardid, M.; Tortosa, D.D.; Felis, I.; Martínez-Mora, J.A.; Llorens, C.D.; Cervantes, P. Acoustic parametric signal generation for underwater communication. *Sensors* **2018**, *18*, 2149. [CrossRef]
19. Campo Valera, M.M.; Felis Enguix, I. Propiedades y Aplicaciones del Efecto Paramétrico en Aire y Agua. IV Jornadas JAAS Acústica, Audio y Sonido 2018. Universidad Tres de Febrero, Buenos Aires, Argentina. 2018. Available online: https://www.jaas.untref.edu.ar/uploads/documents/IV_JAAS-Memorias.pdf (accessed on 23 October 2024).
20. An, J.; Ra, H.; Youn, C.; Kim, K. Experimental results of underwater acoustic communication with nonlinear frequency modulation waveform. *Sensors* **2021**, *21*, 7194. [CrossRef]
21. Zhou, H.; Huang, S.; Li, W. Parametric acoustic array and its application in underwater acoustic engineering. *Sensors* **2020**, *20*, 2148. [CrossRef]
22. Cheng, Y.; Zhao, A.; Hui, J.; An, T.; Zhou, B. Parametric underwater transmission based on pattern time delay shift coding system. *Math. Probl. Eng.* **2018**, *2018*, 8249245. [CrossRef]
23. Ardid, M.; Campo-Valera, M.D.; Tortosa, D.; Felis, I.; Llorens, C.D.; Martínez-Mora, J.A. Underwater communication using acoustic parametric arrays. *Proceedings* **2018**, *2*, 139. [CrossRef]
24. Schneider von Deimling, J.; Held, P.; Feldens, P.; Wilken, D. Effects of using inclined parametric echosounding on sub-bottom acoustic imaging and advances in buried object detection. *Geo-Mar. Lett.* **2016**, *36*, 113–119. [CrossRef]
25. Tan, H.P.; Diamant, R.; Seah, W.K.; Waldmeyer, M. A survey of techniques and challenges in underwater localization. *Ocean. Eng.* **2011**, *38*, 1663–1676. [CrossRef]
26. Wang, C.; Zhu, G.; Tang, S.; Yin, J.; Guo, L.; Sheng, X.; Li, M. Directional bionic underwater communication method using a parametric acoustic array and recursive filtering. *Appl. Acoust.* **2022**, *191*, 108665. [CrossRef]
27. Ortuño-Sáez, G.; Sánchez-Ricart, L. Aliasing Reduction with a 6th Order Space-Time Variational Formulation. *Acta Acust. United Acust.* **2016**, *102*, 1045–1060. [CrossRef]
28. Serrano, E.P.; Fabio, M.; Figliola, A. Métodos tiempo-frecuencia basados en la transformada wavelet. *Rev. Math. Teor. Apl.* **2012**, *19*, 157–168. [CrossRef]
29. Cervenka, P.; Alais, P. Fourier formalism for describing nonlinear self-demodulation of a primary narrow ultrasonic beam. *J. Acoust. Soc. Am.* **1990**, *88*, 473–481. [CrossRef]
30. Diamant, R. Clustering approach for detection and time of arrival estimation of hydroacoustic signals. *IEEE Sens. J.* **2016**, *16*, 5308–5318. [CrossRef]
31. Gezici, S. A Survey on Wireless Position Estimation. *Wirel. Pers. Commun.* **2007**, *44*, 263–282. [CrossRef]
32. Chen, J.; Benesty, J.; Huang, Y. Time Delay Estimation in Room Acoustic Environments: An Overview. *EURASIP J. Adv. Signal Process.* **2006**, *2006*, 26530. [CrossRef]
33. Ash, J.N.; Moses, R.L. Acoustic time delay estimation and sensor network self-localization: Experimental results. *J. Acoust. Soc. Am.* **2005**, *118*, 841–850. [CrossRef]
34. McCrady, D.; Doyle, L.; Forstrom, H.; Dempsey, T.; Martorana, M. Mobile ranging using low-accuracy clocks. *IEEE Trans. Microw. Theory Tech.* **2000**, *48*, 951–958. [CrossRef]
35. Pallas, M.A.; Jourdain, G. Active high resolution time delay estimation for large BT signals. *IEEE Trans. Signal Process.* **1991**, *39*, 781–788. [CrossRef]
36. Cheng, L.; Liu, Y.; Zhang, B.; Hu, Z.; Zhu, H.; Luo, B. Direction of Arrival Joint Prediction of Underwater Acoustic Communication Signals Using Faster R-CNN and Frequency–Azimuth Spectrum. *Remote Sens.* **2024**, *16*, 2563. [CrossRef]
37. Zhang, Y.; Huang, Y.; Tao, J.; Tang, S.; So, H.C.; Hong, W. A Two-Stage Multi-Layer Perceptron for High-Resolution DOA Estimation. *IEEE Trans. Veh. Technol.* **2024**, *73*, 9616–9631. [CrossRef]
38. Feintuch, S.; Tabrikian, J.; Bilik, I.; Permuter, H. Neural-Network-Based DOA Estimation in the Presence of Non-Gaussian Interference. *IEEE Trans. Aerosp. Electron. Syst.* **2024**, *60*, 119–132. [CrossRef]
39. Guo, Y.; Zhang, Z.; Huang, Y. Dual Class Token Vision Transformer for Direction of Arrival Estimation in Low SNR. *IEEE Signal Process. Lett.* **2024**, *31*, 76–80. [CrossRef]
40. Papageorgiou, G.; Sellathurai, M.; Eldar, Y. Deep Networks for Direction-of-Arrival Estimation in Low SNR. *IEEE Trans. Signal Process.* **2021**, *69*, 3714–3729. [CrossRef]

41. Zheng, S.; Yang, Z.; Shen, W.; Zhang, L.; Zhu, J.; Zhao, Z.; Yang, X. Deep Learning-Based DOA Estimation. *IEEE Trans. Cogn. Commun. Netw.* **2024**, *10*, 819–835. [CrossRef]
42. Merkofer, J.P.; Revach, G.; Shlezinger, N.; Routtenberg, T.; van Sloun, R.J.G. DA-MUSIC: Data-Driven DoA Estimation via Deep Augmented MUSIC Algorithm. *IEEE Trans. Veh. Technol.* **2024**, *73*, 2771–2785. [CrossRef]
43. Bell, C.J.; Adhikari, K.; Freeman, L.A. Convolutional Neural Network-Based Regression for Direction of Arrival Estimation. In Proceedings of the 2023 IEEE 14th Annual Ubiquitous Computing, Electronics & Mobile Communication Conference (UEMCON), New York, NY, USA, 12–14 October 2023; IEEE: Piscataway, NJ, USA, 2023; Volume I, pp. 0373–0379. [CrossRef]
44. Campo-Valera, M.; Villó-Pérez, I.; Fernández-Garrido, A.; Rodríguez-Rodríguez, I.; Asorey-Cacheda, R. Exploring the Parametric Effect in Nonlinear Acoustic Waves. *IEEE Access* **2023**, *11*, 97221–97238. [CrossRef]
45. Oppenheim, A.V.; Schafer, R.W. *Tratamiento de señales en Tiempo Discreto*; Prentice Hall: Old Tappan, NJ, USA, 2011.
46. Youn, D.; Mathews, V. Adaptive realizations of the maximum likelihood processor for time delay estimation. *IEEE Trans. Acoust. Speech Signal Process.* **1984**, *32*, 938–940. [CrossRef]
47. Knapp, C.; Carter, G. The generalized correlation method for estimation of time delay. *IEEE Trans. Acoust. Speech Signal Process.* **1976**, *24*, 320–327. [CrossRef]
48. Cabot, R. A note on the application of the Hilbert transform to time delay estimation. *IEEE Trans. Acoust. Speech Signal Process.* **1981**, *29*, 607–609. [CrossRef]
49. Choi, H.I.; Williams, W. Improved time-frequency representation of multicomponent signals using exponential kernels. *IEEE Trans. Acoust. Speech Signal Process.* **1989**, *37*, 862–871. [CrossRef]
50. Serrano, E.G.F.; Cardona i Foix, S.; Nebot, L.J. Análisis en tiempo y frecuencia de señales de vibración tomadas al pie del carril durante el paso de un tren. *Sci. Tech.* **2007**, *13*, 243–247.
51. Calleja, B.; del Río, L.; San Emeterio, J.L. Procesado digital de señales ultrasónicas para la determinación de constantes elásticas dinámicas en materiales rocosos. In *Acustica 2008: V Congreso Ibérico de Acústica, XXXIX Congreso Español de Acústica TecniAcustica 2008, Acoustics European Symposium, ExpoAcustica 2008*; Sociedad Española de Acústica (SEA): Coimbra, Portugal, 2008; pp. 1–12.
52. Adrián-Martínez, S.; Bou-Cabo, M.; Felis, I.; Llorens, C.D.; Martínez-Mora, J.A.; Saldaña, M.; Ardid, M. Acoustic Signal Detection Through the Cross-Correlation Method in Experiments with Different Signal to Noise Ratio and Reverberation Conditions. In *Ad-Hoc Networks and Wireless*; Garcia Pineda, M., Lloret, J., Papavassiliou, S., Ruehrup, S., Westphall, C.B., Eds.; Springer: Berlin/Heidelberg, Germany, 2015; pp. 66–79. [CrossRef]
53. Campo-Valera, M.; Rodríguez-Rodríguez, I.; Rodríguez, J.V.; Herrera-Fernández, L.J. Proof of Concept of the Use of the Parametric Effect in Two Media with Application to Underwater Acoustic Communications. *Electronics* **2023**, *12*, 3459. [CrossRef]
54. Campo-Valera, M.; Diego-Tortosa, D.; Asorey-Cacheda, R.; Gómez-Tornero, J.; Herrera-Fernández, L. A Novel Modulation Approach Based on Nonlinear Acoustic Signals for Underwater Communications. In Proceedings of the 10th Convention of the European Acoustics Association Forum Acusticum 2023, Torino, Italy, 11–15 September 2023; European Acoustics Association: Torino, Italy, 2023; pp. 5065–5070. [CrossRef]
55. Enflo, B.O.; Hedberg, C.M. *Theory of Nonlinear Acoustics in Fluids*, 2002nd ed.; Fluid Mechanics and Its Applications; Springer: New York, NY, USA, 2002.
56. Tjo/tta, J.N.; Tjo/tta, S. Nonlinear equations of acoustics, with application to parametric acoustic arrays. *J. Acoust. Soc. Am.* **1981**, *69*, 1644–1652. [CrossRef]
57. Kinsler, L.E.; Frey, A.R.; Coppens, A.B.; Sanders, J.V. *Fundamentals of Acoustics*, 4th ed.; John Wiley & Sons: Nashville, TN, USA, 1999.

Disclaimer/Publisher's Note: The statements, opinions and data contained in all publications are solely those of the individual author(s) and contributor(s) and not of MDPI and/or the editor(s). MDPI and/or the editor(s) disclaim responsibility for any injury to people or property resulting from any ideas, methods, instructions or products referred to in the content.